Relativistic effects in the anomalous enhancement of charge radii of new magic isotopes ^{52,54}Ca*

Shan Liu (刘姗)[1,2] Jia Liu (刘佳)[1,2#] Yi-Fei Niu (牛一斐)[1,2,3] Wen-Hui Long (龙文辉)[1,2,3†]

[1]Frontier Science Center for Rare isotope, Lanzhou University, Lanzhou 730000, China
[2]School of Nuclear Science and Technology, Lanzhou University, Lanzhou 730000, China
[3]Joint Department for Nuclear Physics, Lanzhou University and Institute of Modern Physics, CAS, Lanzhou 730000, China

Abstract: The remarkable isotope shift of the charge radius of ^{52}Ca relative to ^{48}Ca presents a significant challenge to the magic nature of $N = 32$. In this work, we aim to clarify this apparent inconsistency by employing the relativistic Hartree-Fock (RHF) theory and the extended configuration interaction RHF (CI-RHF) model. It is shown that calculations with the RHF Lagrangian PKA1 successfully reproduce the energy observables related to nuclear magicity at $N = 32$ and 34, as well as the neutron (ν) orbital radii of $\nu 2p_{3/2}$ and $\nu 1f_{7/2}$ in ^{52}Ca, accounting for approximately 70% of the measured isotope shift of ^{52}Ca. Moreover, it is demonstrated that the isotope shift of the charge radius is mainly driven by the relativistic corrections of nuclear interaction, whereas the spatial extension of the low-l orbit $\nu 2p_{3/2}$ is sensitive to the binding depth. In particular, the relativistic corrections of the interactions between the $\nu 2p$ and s orbits are significant for the opening of the sub-shells $N = 32$ and 34, yet contribute only weakly to enhancing the isotope shift of the charge radius. These results reveal that the anomalous isotope shift and the emergence of the new magicity do not share exactly the same microscopic mechanism, at least within the RHF framework, thereby largely resolving the apparent inconsistency. Our findings highlight the importance of relativistic effects in understanding the novel properties of unstable nuclei.

Keywords: charge radius, Relativistic Hartree-Fock, relativistic effects, Dirac Inversion Partners

DOI: 10.1088/1674-1137/ae7dbf **CSTR:** 32044.14.ChinesePhysicsC.50091002

The global progress in rare isotope beam facilities and nuclear detectors has revealed a wealth of nuclear novel phenomena, including the emergence of new magic shells [1−4] and the disappearance of traditional ones [5, 6]. This significantly enriches our understanding of nuclear magicity, a fundamental aspect of nuclear physics. Particularly, two new sub-shells have been identified in neutron-rich Ca isotopes, namely $N = 32$ in ^{52}Ca and $N = 34$ in ^{54}Ca [3, 4, 7], in addition to the doubly magic ^{40,48}Ca. These findings have drawn considerable interests from both experimental and theoretical perspectives, offering new insights into the magic nature that extends from the stable nuclei to the unstable ones [4, 7−10].

As one of the indicators of nuclear magicity, a sudden increase in charge radii beyond the magic shell is typically observed, as well demonstrated in the Ni [11] and Pb [12] isotopes. However, despite the magic nature of $N = 32$ in ^{52}Ca [3, 4], an anomalous increase in charge radii was continuously observed from ^{48}Ca to ^{52}Ca [13]. A similar trend is also evident from ^{47}K to ^{51}K [11, 14, 15], given that the magicity of $N = 32$ has also been confirmed in ^{51}K [16]. Moreover, the measured spatial extension of neutron orbits in ^{52}Ca also shows an anomalous enhancement of 0.61(23) fm of the root-mean-square (r.m.s) radii of the neutron (ν) orbits $\nu 2p_{3/2}$ compared to $\nu 1f_{7/2}$ [17]. Regarding the magic nature of $N = 32$, it is challenging to understand the anomalous increase of both charge radius and orbital radius of $\nu 2p_{3/2}$ of ^{52}Ca, which were expected to contract slightly under the influence of this magicity.

In parallel, a series of theoretical investigations have been carried out to clarify the global tendency of the charge radii of Ca isotopes. A comparison was made between the experimental data and the *ab-initio* calculations based on realistic Hamiltonians, which incorporate the two-body and three-body potentials, whereas the charge radii were underestimated for the Ca isotopes with $N > 28$ [18]. Within the framework of nuclear density functional theory, the Fayans functional has been re-optimized to reasonably describe the charge radii in the cal-

Received 10 April 2026; Accepted 16 June 2026; Accepted manuscript online 17 June 2026

* This work is partly supported by the Fundamental Research Funds for the Central Universities (lzujbky-2023-stlt01), the National Natural Science Foundation of China (12275111), the National Key Research and Development (R&D) Program (2021YFA1601500), and the Supercomputing Center of Lanzhou University

† E-mail: longwh@lzu.edu.cn

# These authors contributed equally as the first authors

cium neighboring region by integrating data from neutron-rich Ca isotopes [19]. Additionally, a modified relativistic mean field (RMF) plus BCS* theory, which includes a semi-microscopic correction derived from the Cooper pair condensation, has been developed to reproduce the overall trend of the charge radii of Ca isotopes [20]. Nevertheless, resolving the inconsistency between the anomalous increase in the charge radius and the magic nature of ^{52}Ca remains an open issue [13, 15].

As well known, both the spin-orbit (SO) and tensor forces play a significant role in determining nuclear shell evolutions [8, 21, 22] and the emergence of new magic shells [4, 9]. Due to the relativistic scheme and the inclusion of Fock terms, the relativistic Hartree-Fock (RHF) theory [23−25] naturally incorporates both the SO and tensor forces [26−29]. By incorporating the density-dependent meson-nucleon coupling strengths, the RHF effective Lagrangians PKOi ($i = 1,2,3$) [21, 24] and PKA1 [25] have been developed, achieving similar quantitative precision as popular nuclear models on the description of nuclear structure properties. In particular, the RHF theory with PKA1 [25] successfully reproduces the subshells of interest, namely $N = 32$ in ^{52}Ca and $N = 34$ in ^{54}Ca [9, 10]. This unified description arises from the strong couplings between the Dirac inversion partners (DIPs) $\nu 2p_{1/2}$ and $s_{1/2}$ with same angular momentum j but opposite parity [10]. Notably, the exchange degrees of freedom in PKA1, namely the π-pseudo-vector (π-PV) and the ρ-tensor (ρ-T) couplings which contribute almost entirely via the Fock terms, change significantly the in-medium balance between nuclear attractions and repulsions from popular RMF models [30]. This is essential for capturing the strong couplings between the DIPs, which leads to a significant SO splitting of $\nu 2p$ in ^{52}Ca, while resulting in a reduced splitting in ^{54}Ca, in a consistent manner [10].

Recently, the RHF theory has been extended to incorporate configuration interactions beyond the mean field, namely the configuration-interaction RHF (CI-RHF) model [31]. Without introducing any new parameters, by using the effective Hamiltonian derived from the existing RHF Lagrangians, the CI-RHF model attains a quantitative precision similar to that of the conventional shell model in describing the low-lying excitation properties [31, 32]. In particular, with the use of PKA1, the characteristics of the island of inversion exhibited by ^{32}Mg, including the deformation and the low-lying excitation energies, have been successfully reproduced through the applications of the axially deformed relativistic Hartree-Fock-Bogoliubov model [33] and the CI-RHF model [32]. It has been demonstrated that the exchange degrees of freedom associated with the π-PV and ρ-T couplings play a crucial role in determining both the configuration interactions and the binding of ^{32}Mg [32]. The successes achieved by the RHF theory and its extensions [9, 10, 30, 32] motivate us to resolve the inconsistency between the anomalous enhancement of charge radius and the magic nature of ^{52}Ca.

In the context of relativity, the Dirac spinor, which is regarded as the relativistic wave function, consists of upper and lower components. Referring to the non-relativistic form of wave function, the lower component of the Dirac spinor can be seen as a relativistic correction. Consequently, the relativistic nuclear interactions can be decomposed as,

$$V = V_{++} + V_R, \tag{1}$$

where the V_{++} term corresponds to the part contributed solely by the upper (+) components, and the remaining part denoted as the V_R term represents a relativistic correction of nuclear interaction. It is worth noting that, due to the relativistic representation of nuclear interactions, mainly the interplay between the Lorentz scalar and vector couplings, repulsive V_R terms are typically obtained [10].

As generally recognized, nuclear force consists of central, SO and tensor type contributions. While it is challenging to separate these individual components in a relativistic nuclear interaction. By applying non-relativistic reduction, one can approximately extract the tensor force components carried by the π-PV and ρ-T couplings [9, 21, 23, 27, 29]. In order to precisely identify the central, SO and tensor contributions in a relativistic effective interaction, we adopt a numerical yet exact recipe, namely the spin-tensor decomposition method [34−39].

For fermions (e.g., nucleon) with spin 1/2, one can construct a complete set of the linear operators in a two-particle spin space from their spin operators as [34, 36],

$$\begin{aligned} &S_1^{(0)} = 1, && S_2^{(0)} = [\sigma_1 \otimes \sigma_2]^{(0)}, \\ &S_3^{(1)} = \sigma_1 + \sigma_2, && S_4^{(2)} = [\sigma_1 \otimes \sigma_2]^{(2)}, \\ &S_5^{(1)} = [\sigma_1 \otimes \sigma_2]^{(1)}, && S_6^{(1)} = \sigma_1 - \sigma_2. \end{aligned} \tag{2}$$

Thus, the two-body interaction can be expressed as

$$V = \sum_{k=0,1,2} V^{(k)} = \sum_{k=0,1,2} S^{(k)} \otimes Q^{(k)}. \tag{3}$$

In this context, $V^{(0)}$, $V^{(1)}$ and $V^{(2)}$ correspond to the central, SO and tensor parts of the effective nucleon-nucleon interaction, respectively. Under the LS coupled scheme, the k-th ($k = 0,1,2$) order terms of the two-body interaction matrix elements are extracted as,

$$\langle (ab):LS,JM|V^{(k)}|(cd):L'S',JM\rangle = \hat{k}^2\sum_{J'}\hat{J}'^2\mathcal{D}^{JJ',k}_{LS,L'S'}\langle (ab):LS,J'M|V|(cd):L'S',J'M\rangle, \tag{4}$$

where a, b, c, and d denote specific single-particle states, $\hat{k}^2 = 2k+1$, and $\hat{J}'^2 = 2J'+1$. The symbol $\mathcal{D}$ is expressed as follows:

$$\mathcal{D}^{JJ',k}_{LS,L'S'} = (-1)^{J+J'}\begin{Bmatrix} L & S & J \\ S' & L' & k \end{Bmatrix}\begin{Bmatrix} L & S & J' \\ S' & L' & k \end{Bmatrix}. \tag{5}$$

In essence, such a decomposition holds significant potential for numerically extracting the central, spin-orbit, and tensor components of the two-body interaction, provided that a sufficiently complete set of interaction matrix elements is available. Specifically, the spin-tensor decomposition provides insight into the relativistic correction of the nuclear interaction, particularly the V_R term. Furthermore, it is anticipated that an intuitive understanding will emerge for interactions between the DIPs, which are augmented by the V_R terms and play a crucial role in the opening of sub-shells at $N = 32$ and 34 [10].

The existence of nuclear magicity can be substantiated by systematic trends in charge radius. In this study, the charge radius r_{ch} is computed by accounting for the finite-size effect of protons and the intrinsic charge distribution of neutrons, expressed as $r^2_{ch} = r^2_p + 0.862^2 - 0.336^2 N/Z$. Here, r_p denotes the root mean-square (r.m.s) radius of point-like protons, with the proton radius being 0.862 fm [40], the neutron charge radius being 0.336 fm [41], and neutron number N and proton one Z. To enable a quantitative comparison between experimental and theoretical results, the differential charge radii along the isotopic chain, specifically the isotope shift $\delta\langle r^2\rangle$ of the charge radius, are introduced as follows.

$$\delta\langle r^2\rangle_{A,A'} = \langle r^2_{ch}\rangle_{A'} - \langle r^2_{ch}\rangle_A, \tag{6}$$

where A and A' denote the mass numbers of the isotopes. For the Ca isotopes, ^{48}Ca is considered the reference isotope, hence $A = 48$. For simplicity, the subscript of $\delta\langle r^2\rangle$ will be omitted hereafter.

In this study, spherical symmetry is imposed on the even Ca isotopes ranging from $N = 26$ to $N = 36$ in the RHF calculations. The pairing correlations are evaluated using the BCS scheme with the finite-range part of the Gogny force D1S [42] as the pairing interaction. To elucidate the mechanism underlying the anomalous charge radius, the RHF effective Lagrangians PKA1 [25], PKO2, and PKO3 [21] are employed. These are compared with the RMF Lagrangians, specifically DD-ME2 [43], PK1 [44], and NL3 [45]. For the CI-RHF calculations, the effective Hamiltonians are derived consistently from the selected RHF Lagrangians [31]. The neutron valence space is defined as the *pf* shell on top of the frozen core of ^{40}Ca.

It is well established that the filter function, $\delta e = S_{2n}(N) - S_{2n}(N+1)$, and the two-neutron energy gap, $\Delta_{2n} = S_{2n}(N) - S_{2n}(N+2)$–where S_{2n} represents the two-neutron separation energy–along with the energy of the excited state 2^+_1, provide quantifiable criteria for identifying nuclear magicity. To provide a comprehensive analysis, both the RHF and CI-RHF calculations were performed for the even isotopes $^{48\sim56}$Ca using the Lagrangians PKA1, PKO2, and PKO3. Figure 1 displays the two-neutron energy gaps Δ_{2n} (MeV) and the excitation energy $E(2^+_1)$ (MeV) obtained from the RHF and CI-RHF calculations, respectively.

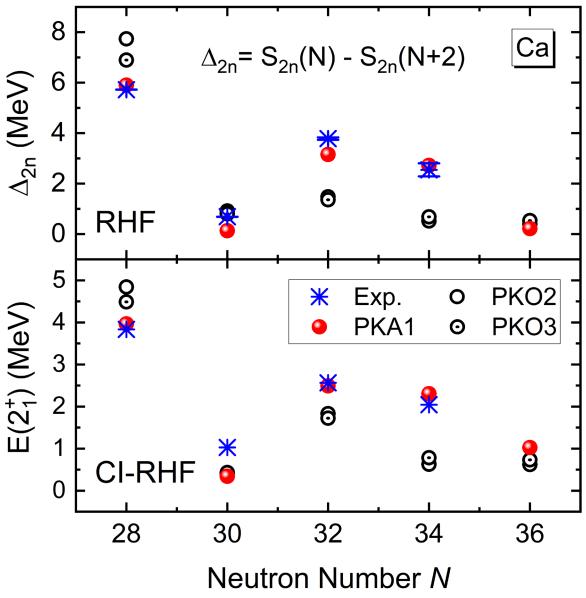

Fig. 1. (color online) Two-neutron energy gaps Δ_{2n} (MeV) and the excitation energies $E(2^+_1)$ (MeV) of the even isotopes $^{48\sim56}$Ca calculated by PKA1, PKO2 and PKO3, in comparison with the experimental data [3, 4, 7, 46].

As illustrated in Fig. 1, the values of Δ_{2n} and $E(2^+_1)$ predicted by PKA1 are in excellent agreement with experimental data [3, 4, 7, 46], particularly for the doubly magic nucleus ^{48}Ca and the newly identified magic isotopes ^{52,54}Ca. In contrast, both PKO2 and PKO3 underestimate Δ_{2n} and $E(2^+_1)$ values for ^{52,54}Ca. It is noteworthy that the filter functions δe, another energy observable used to assess nuclear magicity at $N = 32$ and 34, are also accurately reproduced by PKA1 [10]. These findings underscore the predictive capability of the RHF Lagrangian PKA1 in capturing nuclear shell effects at both the mean-

field level and beyond, specifically in the RHF and extended CI-RHF models. This capability is crucial for further elucidating the underlying mechanism of the anomalous charge radius of ^{52}Ca.

Taking ^{48}Ca as the reference, the isotope shift of the charge radius is determined for ^{52}Ca, as shown in Eq. (6). Table 1 presents the $\delta\langle r^2\rangle$ values (fm^2) extracted from the RHF calculations, along with results from selected RMF models. Compared to the experimental value $\delta\langle r^2\rangle^{\rm Exp.} = 0.530 \pm 0.012$ fm^2 [13, 47], all the selected models underestimate the isotope shift for ^{52}Ca to varying degrees. Notably, extending beyond the mean-field level, the results are not significantly altered, as indicated by the CI-RHF calculations, which are not shown here.

Table 1. Isotope shift of charge radius $\delta\langle r^2\rangle$ (fm^2) of ^{46,50,52,54}Ca given by the RHF Lagrangians PKA1 [25], PKO2 and PKO3 [21], and the RMF ones DD-ME2 [43], PK1 [44] and NL3 [45], by taking ^{48}Ca as the reference. The experimental values are taken from Refs. [13, 47].

	Exp.	PKA1	PKO2	PKO3	DD-ME2	PK1	NL3
^{46}Ca	0.125	0.077	−0.040	−0.020	−0.023	−0.025	−0.020
	–	62%	−32%	−16%	−18%	−20%	−16%
^{50}Ca	0.290	0.207	0.161	0.173	0.168	0.126	0.142
	–	71%	56%	60%	58%	43%	49%
^{52}Ca	0.530	0.376	0.346	0.342	0.336	0.253	0.244
	–	71%	65%	65%	63%	48%	46%
^{54}Ca	–	0.564	0.577	0.528	0.521	0.393	0.388

More specifically, regarding the experimental data, the RHF and RMF models reproduce the isotope shift $\delta\langle r^2\rangle$ of charge radii from ^{48}Ca to ^{52}Ca, averaging approximately 67% and 52%, respectively. Among the selected models, the best agreement is achieved with PKA1, which accounts for about 70% of the experimental isotope shift [13, 47]. Notably, PKA1 also predicts a distinct decrease in the charge radii from ^{46}Ca to ^{48}Ca, aligning with the experimental trend. It is evident that PKA1 provides a more accurate description of the kink around the traditional magic number $N = 28$ compared to the other selected effective interactions. Considering its reproduction of energy observables such as Δ_{2n} and $E(2_1^+)$ related to nuclear magicity, the RHF Lagrangian PKA1 is employed for the subsequent systematic investigation.

To elucidate the underlying mechanisms of the anomalous charge radius and the orbital radius of $\nu 2p_{3/2}$, we performed test calculations for ^{52}Ca by selectively excluding the V_R or V_{++} term from the interactions between the neutron valence orbital $\nu 2p_{3/2}$ and other orbitals. The differences between the test calculations and the original calculation for the isotope shift $\delta\langle r^2\rangle$ of the charge radius and the orbital radius r_{nlj} of $\nu 2p_{3/2}$ are defined as $\Delta\langle r^2\rangle = \delta\langle r^2\rangle^{\rm test} - \delta\langle r^2\rangle$ and $\Delta r_{nlj} = r_{nlj}^{\rm test} - r_{nlj}$, respectively. Figures 2(a) and 2(b) present the values of $\Delta\langle r^2\rangle$ (fm^2) and Δr_{nlj} (fm), respectively, where the open (filled) circles represent the test calculations excluding the V_{++} (V_R) terms.

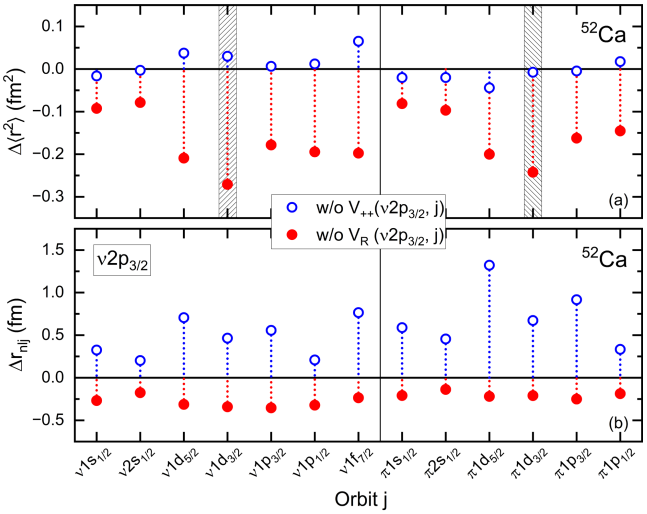

Fig. 2. (color online) Differences between the test and original calculations, namely $\Delta\langle r^2\rangle$ (fm^2) and Δr_{nlj} (fm), respectively for the isotope shift of charge radius $\delta\langle r^2\rangle$ and the orbital radius r_{nlj} of $\nu 2p_{3/2}$ in ^{52}Ca. The results are given by the calculations with PKA1, and the open and filled circles represent the test calculations excluding the V_{++} and V_R terms, respectively.

As demonstrated in Fig. 2(a), excluding the V_R terms results in significant reductions in the isotope shift $\delta\langle r^2\rangle$ of the charge radius for ^{52}Ca. This contrasts with the outcomes obtained from the exclusion of the V_{++} terms but is consistent with theoretical expectations. According to the relativistic representation of nuclear interactions, the V_R terms are generally repulsive [10]. Their exclusion causes the ^{48}Ca core in ^{52}Ca to contract, thereby reducing the isotope shift $\delta\langle r^2\rangle$. Consequently, the unexpected enhancement in the isotope shift of the charge radius can be attributed to the polarization of the valence $2p_{3/2}$ neutrons on the nuclear core. Moreover, such polarization effects are primarily driven by the repulsive relativistic corrections in the interactions between the $\nu 2p_{3/2}$ orbital and the ^{48}Ca core, specifically the V_R terms.

In particular, as shown in Fig. 2(a), relatively weak effects on the isotope shift of the charge radius are observed in the test calculations when excluding the V_R terms in the interactions between s and $\nu 2p_{3/2}$ orbits, in contrast to the other cases. Intuitively, nucleons populating various orbits are displaced outward by the repulsive

V_R terms, resulting in a spatial expansion of charge distributions. However, such effects are expected to be weak for the *s*-orbits, given that *s*-orbital nucleons ($l = 0$) remain in the interior region of the nucleus. In contrast, nucleons in the *p*, *d*, and *f*-orbits, due to centrifugal repulsions, are located on the periphery, and on average, the V_R terms exert substantial effects on the charge radius. In fact, as illustrated in Fig. 2(a), these outcomes exhibit a certain dependence on angular momentum. Notably, the polarization effects from the $\nu 2p_{3/2}$ neutrons are overall considerable, except in the case of *s*-orbits, indicating a generally strong repulsive V_R term.

Conversely, as shown in Fig. 2(b), the orbital radius of $\nu 2p_{3/2}$ appears to be more sensitive to the attractive V_{++} terms than to the repulsive V_R terms. These results may suggest that the enhanced isotope shift of the charge radius in ^{52}Ca is not directly related to the enlargement of the orbital radius of $\nu 2p_{3/2}$. For instance, when excluding the V_{++} term of the interaction between the $\nu 2p_{3/2}$ and proton (π) $\pi 1d_{5/2}$ orbits, the orbital radius r_{nlj} increases notably, yet the isotope shift $\delta\langle r^2\rangle$ decreases slightly. Moreover, as revealed in Ref. [10], the repulsive V_R terms are even more pronounced for the DIPs. Correspondingly, as illustrated in Fig. 2(a), the most substantial reductions of $\delta\langle r^2\rangle$ occur when excluding the V_R terms of the interactions between the $\nu 2p_{3/2}$ orbit and its DIPs, specifically $\nu 1d_{3/2}$ and $\pi 1d_{3/2}$.

Due to its low orbital angular momentum *l*, the spatial distribution of the valence orbit $\nu 2p_{3/2}$ in ^{52}Ca can be sensitive to the binding depth. Indeed, when the attractive V_{++} terms are excluded, the $\nu 2p_{3/2}$ orbit becomes more weakly bound, resulting in significantly enlarged orbital radii, as shown in Fig. 2(b). This observation is consistent with the role of weakly bound *p* orbits in the formation of nuclear halos, such as in the drip-line isotopes of Zr [48]. In contrast, the proton orbits in neutron-rich ^{52}Ca are relatively deeply bound. Consequently, the exclusions of the V_{++} terms have no substantial impact on the isotope shift $\delta\langle r^2\rangle$, as illustrated in Fig. 2(a). It is noteworthy that, in all the test calculations excluding either the V_R or V_{++} terms, the proton orbits of ^{52}Ca remain deeply bound.

As deduced from the above discussions, it is clear that the anomalous charge-radius enhancement and the enlarged $\nu 2p_{3/2}$ orbital radius should be distinguished. The former is primarily due to the polarization of the valence $2p_{3/2}$ neutrons influenced by the repulsive V_R term, whereas the latter is closely associated with the binding depth of the orbit. To more clearly disentangle these two effects, we perform two additional diagnostic test calculations using the PKA1 interaction. In these tests, no new effective interaction is constructed, nor is any refitting conducted. Instead, only the V_{++} and V_R terms of the matrix elements between the $\nu 2p_{3/2}$ orbit and its DIPs, specifically $\nu 1d_{3/2}$ and $\pi 1d_{3/2}$, are multiplied by prescribed factors. These two cases are denoted as $V_{pd}\Uparrow$ and $V_{pd}\Downarrow$, corresponding to $(1.24V_{++}, 1.45V_R)$ and $(0.76V_{++}, 0.55V_R)$, respectively. These factors are chosen numerically so that the single-particle energy of $\nu 2p_{3/2}$ remains close to that obtained in the original PKA1 calculation, as shown in the inset of Fig. 3(a), while the polarization of the valence $2p_{3/2}$ neutrons is enhanced or weakened. Therefore, these calculations should be regarded as sensitivity tests rather than new parameterizations.

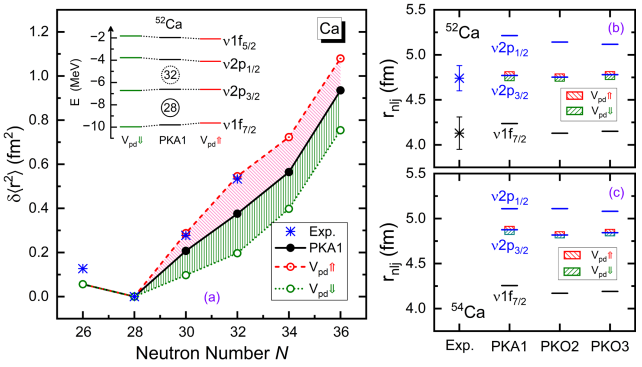

Fig. 3. (color online) Isotope shift $\delta\langle r^2\rangle$ (fm^2) for $^{46\sim56}$Ca [plot (a)] given by PKA1, and the orbital radii r_{nlj} (fm) of $\nu 1f_{7/2}$ and $\nu 2p$ orbits for ^{52}Ca [plot (b)] and ^{54}Ca [plot (c)] given by PKA1, PKO2 and PKO3. See the text for details.

Figure 3(a) presents the isotope shifts $\delta\langle r^2\rangle$ (fm^2) of the charge radius for $^{46\sim56}$Ca obtained from the test and original calculations using PKA1, in comparison with the experimental data [13, 47]. Figures 3(b) and 3(c) display the orbital radii r_{nlj} (fm) of $\nu 1f_{7/2}$ and $\nu 2p$ orbits for ^{52}Ca and ^{54}Ca, respectively. These results are given by the test and original calculations using PKA1, PKO2, and PKO3, in comparison with the available experimental data [17]. As seen from Fig. 3(a), PKA1 produces a substantial enhancement of the isotope shift $\delta\langle r^2\rangle$ of the charge radius from ^{48}Ca to ^{52}Ca and the kink across the magic shell $N = 28$, although the values of $\delta\langle r^2\rangle$ are somewhat underestimated when compared to the data. Further, the isotope shifts $\delta\langle r^2\rangle$ obtained from the test calculations, namely the cases of $V_{\rm pd}\Uparrow$ and $V_{\rm pd}\Downarrow$, differ significantly from the original calculations. Specifically, the former reproduces the enhancement of $\delta\langle r^2\rangle$ from ^{48}Ca to ^{52}Ca. This suggests that the charge radius of ^{52}Ca is very sensitive to the interactions between the $\nu 2p_{3/2}$ orbit and its DIPs, after excluding the influence of the spatial expansion of $\nu 2p_{3/2}$. In conjunction with the results in Fig. 2(a), such an effect originates mainly from the relativistic corrections of the interactions, specifically the repulsive V_R terms. In principle, similar results as Fig. 3(a) can also be obtained by modifying the interactions between the $\nu 2p_{3/2}$ and other orbits like $1d_{5/2}$ and $1f_{7/2}$. Given that the V_R terms of the interactions between the DIPs are much

stronger than other cases [10], it would be preferable to adjust the interactions between the DIPs to test the polarization effects from the $\nu 2p_{3/2}$ neutrons on the charge radius.

Furthermore, as illustrated in Fig. 3(b), PKA1, PKO2, and PKO3 accurately reproduce the orbital radii of $\nu 2p_{3/2}$ and $\nu 1f_{7/2}$ for ^{52}Ca [17]. In contrast, as shown in Figs. 3(b) and 3(c), the orbital radii of $\nu 2p_{3/2}$ do not exhibit significant variation with changes in the interactions between the $\nu 2p_{3/2}$ orbit and its DIPs. This is because the binding depth of $\nu 2p_{3/2}$ remains nearly unchanged compared to the original PKA1 calculations, as depicted in the inset of Fig. 3(a). Thus, when combining Figs. 2 and 3, it can be inferred that the enhancement of the isotope shift $\delta\langle r^2\rangle$ in the charge radius from ^{48}Ca to ^{52}Ca is primarily due to the polarization effects of the valence $2p_{3/2}$ neutrons, which are mediated by the V_R terms of the interactions. This reveals a significant relativistic effect on the charge radius, which is applicable to the further enhancement of the charge radius of ^{54}Ca. Specifically, the valence $\nu 2p_{1/2}$ neutrons in ^{54}Ca also exert similar polarization effects on the charge radius via the V_R terms, resulting in a continuous enhancement of $\delta\langle r^2\rangle$ as depicted in Fig. 3(a).

It is noteworthy that, for reasons similar to those discussed in Fig. 2(a), the strong V_R terms of the couplings between the DIPs $\nu 2p_{1/2}$ and $s_{1/2}$, which are crucial for the opening of the sub-shells $N = 32$ and 34 [10], do not produce significant effects on the charge radius of ^{54}Ca. This suggests that the anomalous isotope shift of the charge radii of ^{52,54}Ca is not directly related to their magic nature. Conversely, it is evident that the orbital radius of $\nu 2p_{3/2}$ is sensitive to binding depth due to its low-l characteristic. To a certain extent, the opening of the sub-shell $N = 32$ results in a relatively high-lying and extended $\nu 2p_{3/2}$ orbit.

As mentioned previously, the isotope-shift enhancement from ^{48}Ca to ^{52}Ca is primarily due to the polarization effects carried by the V_R terms of the interactions between the valence $2p_{3/2}$ neutrons and the core. Interestingly, as highlighted in Ref. [10], the opening of the $N = 32$ and 34 sub-shells is also influenced by the V_R terms of the interactions between the $\nu 2p$ and s orbits. To provide further insight, Figs. 4(a-b) display the spin-tensor decompositions of the V_{++} and V_R terms, namely the V_C, V_{SO}, and V_T components, using the DIPs $(\nu 2s_{1/2},\nu 2p_{1/2})$ and $(\nu 1d_{3/2},\nu 2p_{3/2})$ as representatives. Additionally, Figs. 4(c-d) show the contributions to the SO splittings ΔE_{SO} (MeV) of ^{52}Ca from the orbits $\nu 2s_{1/2}$ and $\nu 1d_{3/2}$, including the total V, V_{++}, and V_R terms.

In Figs. 4(a-b), the V_{++} terms are dominated by attractive central components V_C, which are largely canceled by the repulsive V_C components in the V_R terms. Particularly, the V_R terms are predominant in the SO components V_{SO}. Consistently, as illustrated in Fig. 4(c),

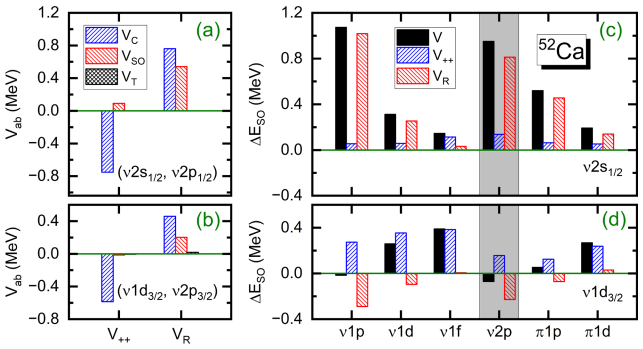

Fig. 4. (color online) Spin-tensor decompositions of the V_{++} and V_R terms in the interactions of the DIPs $(\nu 2s_{1/2},\nu 2p_{1/2})$ [plot (a)] and $(\nu 1d_{3/2},\nu 2p_{3/2})$ [plot (b)], and the contributions to the SO splittings of ^{52}Ca from the $\nu 2s_{1/2}$ [plot (c)] and $\nu 1d_{3/2}$ [plot (d)] orbits. The results are extracted from the RHF calculations with PKA1. See the text for details.

the $\nu 2p$ splitting (highlighted in gray) is significantly enlarged by the couplings with the $\nu 2s_{1/2}$ orbit, especially due to the V_R terms. Conversely, this splitting is slightly reduced by the couplings with the $\nu 1d_{3/2}$ orbit, as the V_R term contributes negatively, opposing the V_{++} term, as shown in Fig. 4(d). It is evident that the opening of the sub-shell $N = 32$, specifically the $\nu 2p$ splitting, is significantly influenced by the couplings with the s-orbits, particularly the DIPs $(s_{1/2},\nu 2p_{1/2})$ [10]. However, as illustrated in Figs. 2(a) and 3(a), the enhancements of the isotope shift $\delta\langle r^2\rangle$ originate from the polarization effects of the $2p$ neutrons on the core orbits, excluding the s-orbits. Thus, the enhancements of $\delta\langle r^2\rangle$ from ^{48}Ca to ^{52}Ca, and further to ^{54}Ca, do not share the exact mechanism as the emergence of new magic numbers at $N = 32$ and 34. In other words, although both phenomena involve strong V_R terms in relativistic interactions, the specific ways in which they exert influence are microscopically different, at least within the RHF framework.

In summary, the anomalous isotope shift of the charge radius, along with the neutron orbital radii and the magic nature, is investigated for the novel magic isotopes ^{52}Ca and ^{54}Ca using the relativistic Hartree-Fock (RHF) theory and the extended configuration interaction RHF (CI-RHF) model. The RHF and CI-RHF calculations, utilizing the RHF Lagrangian PKA1, exhibit excellent agreement with experimental data on the energy observables related to nuclear magicity for ^{52,54}Ca. Moreover, the RHF theory with PKA1 accurately reproduces the orbital radii of $\nu 2p_{3/2}$ and $\nu 1f_{7/2}$ for ^{52}Ca and accounts for approximately 70% of the isotope shift in the charge radius of ^{52}Ca relative to ^{48}Ca.

In a series of test calculations, it has been demonstrated that the anomalous isotope shift in the charge radius $\delta\langle r^2\rangle$ of ^{52}Ca arises from the polarization effects of the $\nu 2p_{3/2}$ neutrons on the core orbits, excluding the s orbits. These polarizations are primarily mediated by the relativ-

istic correction term V_R in the interactions. Considering that the couplings between the s and $\nu 2p$ orbits play a crucial role in opening the sub-shells at $N = 32$ and 34, it can be inferred that the anomalous isotope shift $\delta\langle r^2\rangle$ and the emergence of new magicity in ^{52,54}Ca do not entirely share the same microscopic mechanism, at least within the RHF framework. These findings provide a microscopic explanation for the apparent discrepancy between the anomalous isotope shift in the charge radius and the magicity of $N = 32$ in ^{52}Ca. They highlight the importance of relativistic corrections in nuclear interactions and offer new insights into the exotic properties of unstable nuclei. Additionally, due to the low angular momentum, the spatial expansion of the $\nu 2p_{3/2}$ orbit is influenced by its binding depth.

References

[1] A. Ozawa, T. Kobayashi, T. Suzuki *et al*., Phys. Rev. Lett. **84**, 5493 (2000)
[2] D. Warner, Nature **430**, 517 (2004)
[3] F. Wienholtz, D. Beck, K. Blaum *et al*., Nature **498**, 346 (2013)
[4] D. Steppenbeck, S. Takeuchi, N. Aoi *et al*., Nature **502**, 207 (2013)
[5] T. Motobayashi, Y. Ikeda, K. Ieki *et al*., Phys. Lett. B **346**, 9 (1995)
[6] B. Bastin, S. Grévy, D. Sohler *et al*., Phys. Rev. Lett. **99**, 022503 (2007)
[7] S. Michimas, M. Kobayashi, Y. Kiyokawa *et al*., Phys. Rev. Lett. **121**, 022506 (2018)
[8] T. Otsuka, T. Suzuki, R. Fujimoto *et al*., Phys. Rev. Lett. **95**, 232502 (2005)
[9] J. J. Li, J. Margueron, W. H. Long *et al*., Phys. Lett. B **753**, 97 (2016)
[10] J. Liu, Y. F. Niu, and W. H. Long, Phys. Lett. B **806**, 135524 (2020)
[11] F. Sommer, K. König, D. M. Rossi *et al*., Phys. Rev. Lett. **129**, 132501 (2022)
[12] M. Bhuyan, B. Maheshwari, H. A. Kassim *et al*., J. Phys. G: Nucl. Part. Phys. **48**, 075105 (2021)
[13] R. F. G. Ruiz, M. L. Bissell, K. Blaum *et al*., Nat. Phys. **12**, 594 (2016)
[14] K. Kreim, M. L. Bissell, J. Papuga *et al*., Phys. Lett. B **731**, 97 (2014)
[15] Á. Koszorús, X. F. Yang, W. G. Jiang *et al*., Nat. Phys. **17**, 439 (2021)
[16] M. Rosenbusch, P. Ascher, D. Atanasov *et al*., Phys. Rev. Lett. **114**, 202501 (2015)
[17] M. Enciu, H. N. Liu, A. Obertelli *et al*., Phys. Rev. Lett. **129**, 262501 (2022)
[18] V. Somà, P. Navrátil, F. Raimondi *et al*., Phys. Rev. C **101**, 014318 (2020)
[19] M. Kortelainen, Z. H. Sun, G. Hagen *et al*., Phys. Rev. C **105**, L021303 (2022)
[20] R. An, L. S. Geng, and S. S. Zhang, Phys. Rev. C **102**, 024307 (2020)
[21] W. H. Long, H. Sagawa, J. Meng *et al*., Europhys. Lett. **82**, 12001 (2008)
[22] L. J. Wang, J. M. Dong, and W. H. Long, Phys. Rev. C **87**, 047301 (2013)
[23] A. Bouyssy, J. F. Mathiot, N. V. Giai *et al*., Phys. Rev. C **36**, 380 (1987)
[24] W. H. Long, N. V. Giai, and J. Meng, Phys. Lett. **B 640**, 150 (2006)
[25] W. H. Long, H. Sagawa, N. V. Giai *et al*., Phys. Rev. C **76**, 034314 (2007)
[26] L. J. Jiang, S. Yang, J. M. Dong *et al*., Phys. Rev. C **91**, 025802 (2015a)
[27] L. J. Jiang, S. Yang, B. Y. Sun *et al*., Phys. Rev. C **91**, 034326 (2015b)
[28] Y. Y. Zong and B. Y. Sun, Chin. Phys. C **42**, 024101 (2018)
[29] Z. H. Wang, Q. Zhao, H. Z. Liang *et al*., Phys. Rev. C **98**, 034313 (2018)
[30] J. Geng, J. J. Li, W. H. Long *et al*., Phys. Rev. C **100**, 051301 (2019)
[31] J. Liu, Y. F. Niu, and W. H. Long, Chin. Phys. C **49**, 064104 (2025)
[32] Y. Peng, J. Liu, J. Geng *et al*., Chin. Phys. C **49**, 064112 (2025)
[33] J. Geng and W. H. Long, Phys. Rev. C **105**, 034329 (2022)
[34] M. W. Kirson, Phys. Lett. B **47**, 110 (1973)
[35] K. Klingenbeck, Phys. Rev. C **15**, 831 (1977)
[36] Y. Kenji, Nucl. Phys. A **333**, 67 (1980)
[37] B. A. Brown, W. A. Richter, R. E. Julies *et al*., Ann. of Phys. **182**, 191 (1988)
[38] E. Osnes and D. Strottman, Phys. Rev. C **45**, 662 (1992)
[39] N. A. Smirnova, B. Bally, K. Heyde *et al*., Phys. Lett. B **686**, 109 (2010)
[40] A. Grinin, A. Matveev, D. C. Yost *et al*., Science **370**, 1061 (2020)
[41] H. Atac, M. Constantinou, Z. E. Meziani *et al*., Nat. Comm. **12**, 1759 (2021)
[42] J. F. Berger, M. Girod, and D. Gogny, Nucl. Phys. A **428**, 23 (1984)
[43] G. A. Lalazissis, T. Niksic, D. Vretenar *et al*., Phys. Rev. C **71**, 024312 (2005)
[44] W. H. Long, J. Meng, N. V. Giai *et al*., Phys. Rev. C **69**, 034319 (2004)
[45] G. A. Lalazissis, J. König, and P. Ring, Phys. Rev. C **55**, 540 (1997)
[46] M. Wang, W. J. Huang, F. G. Kondev *et al*., Chin. Phys. C **45**, 030003 (2021)
[47] I. Angeli and K. P. Marinova, At. Data Nucl. Data Tables **99**, 69 (2013)
[48] J. Meng and P. Ring, Phys. Rev. Lett. **80**, 460 (1998)